Pergamon

Journal of Structural Geology, Vol. 19, Nos 3–4, pp. 443 to 461, 1997

0191-8141/97 $17.00 + 0.00

PII: S0191-8141(96)00103-4

Bed-by-bed fold growth by kink-band migration: Sant Llorenç de Morunys, eastern Pyrenees

JOHN SUPPE

Department of Geosciences, Princeton University, Princeton, NJ 08544, U.S.A.

and

FRANCESC SÀBAT, JOSEP ANTON MUÑOZ, JOSEP POBLET, EDUARD ROCA and JAUME VERGÉS

Departament de Geologia Dinàmica, Geofísica i Paleontologia, Universitat de Barcelona, Zona Universitària de Pedralbes, 08071 Barcelona, Spain

(*Received* 5 *February* 1996; *accepted in revised form* 12 *November* 1996)

Abstract—Growth strata deposited over and against the flank of the Sant Llorenç de Morunys fold during its final stages of deformation have been mapped at high resolution as the basis for unraveling the kinematics of fold growth. We use restoration techniques based on normal balancing assumptions to decipher the detailed kinematic history of folding. The progressive restorations, as well as balanced forward modeling, show that the last few hundred meters of fold growth were dominated by kink-band migration of a sort that is typical of much fault-related folding. The kink-band migration has produced complex anticlinal hinge-zone geometry, including segmented fold hinges linked by disconformities and unconformities, which has direct and detailed explanation in terms of fluctuations in deposition rate relative to curved-hinge kink-band migration rate. Large fluctuations in the convolution of non-steady sedimentation and deformation are demonstrated, although the absolute fluctuations in deformation and sedimentation are unknown. At a length scale of 100 m, kink-band migration with little or no deposition is interspersed with sedimentation with little or no deformation. At the length scale of 500 m, deposition ranges from 200% to 50% of uplift. © 1997 Elsevier Science Ltd. All rights reserved.

INTRODUCTION

Growth strata, which are strata deposited over the top or against the flanks of growing structures, offer us the possibility of deciphering their kinematic histories. For example, the two cross-sections in the bottom of Fig. 1 have identical final shapes, as shown by the pre-growth strata, and have identical stratigraphy. They only differ in the shape of the growth strata in the fold limb, which tells us they have very different kinematic histories.

Given the sequence of layer shapes we can decipher much or all of the kinematic history of such structures through the process of balanced restoration. The kinematic information is recorded in the spatial distribution of thicknesses and dips. For example, the cross-section on the left formed by kink-band migration; this is shown by the fact that the thickness change in each growth bed is localized in the anticlinal hinge and the fold limb does not vary in dip except in the zone of hinge formation at shallow depths. In contrast the right-hand cross-section formed by limb rotation, which is recorded by the fact that thickness change in each growth bed is spread out over the fold limb, which causes the fold limb to progressively change dip. The contrasting kinematics of the two sections is illustrated at the top of Fig. 1, showing the folding histories of a typical growth bed, in this case the first growth layer. It is the distinctive sequences of layer shapes and thickness variations that record the kinematics.

There are two basic strategies for deciphering fold and fault kinematics from the shapes of growth strata: (i) balanced forward kinematic modeling; and (ii) balanced restoration. Suites of forward models, such as the cross-sections of Fig. 1, are compared with actual structures to identify possible models of their origin; once a viable hypothesis for the structure is generated a new forward model can be 'tailor made' to match the essential details of the actual structure (Mount *et al.*, 1990). In contrast, restoration involves progressive or one-step unfolding and unfaulting of the actual data, subject to balancing constraints (Nunns, 1991; Medwedeff, 1992). The fold kinematics falls out of the balanced restoration as a result of the spatial variation of dips and thicknesses within the growth strata. In this paper we will use a combination of forward modeling and restoration.

Most attempts at using growth strata to decipher kinematics have been rather large scale, focusing on the overall motion of fold growth and fault slip in single structures or even on a regional scale. Here we attempt to move closer to a bed-by-bed understanding of the growth of structures, which raises some significant new issues, including (1) the role of deformational and depositional events in shaping bed-scale growth structure and (2) the

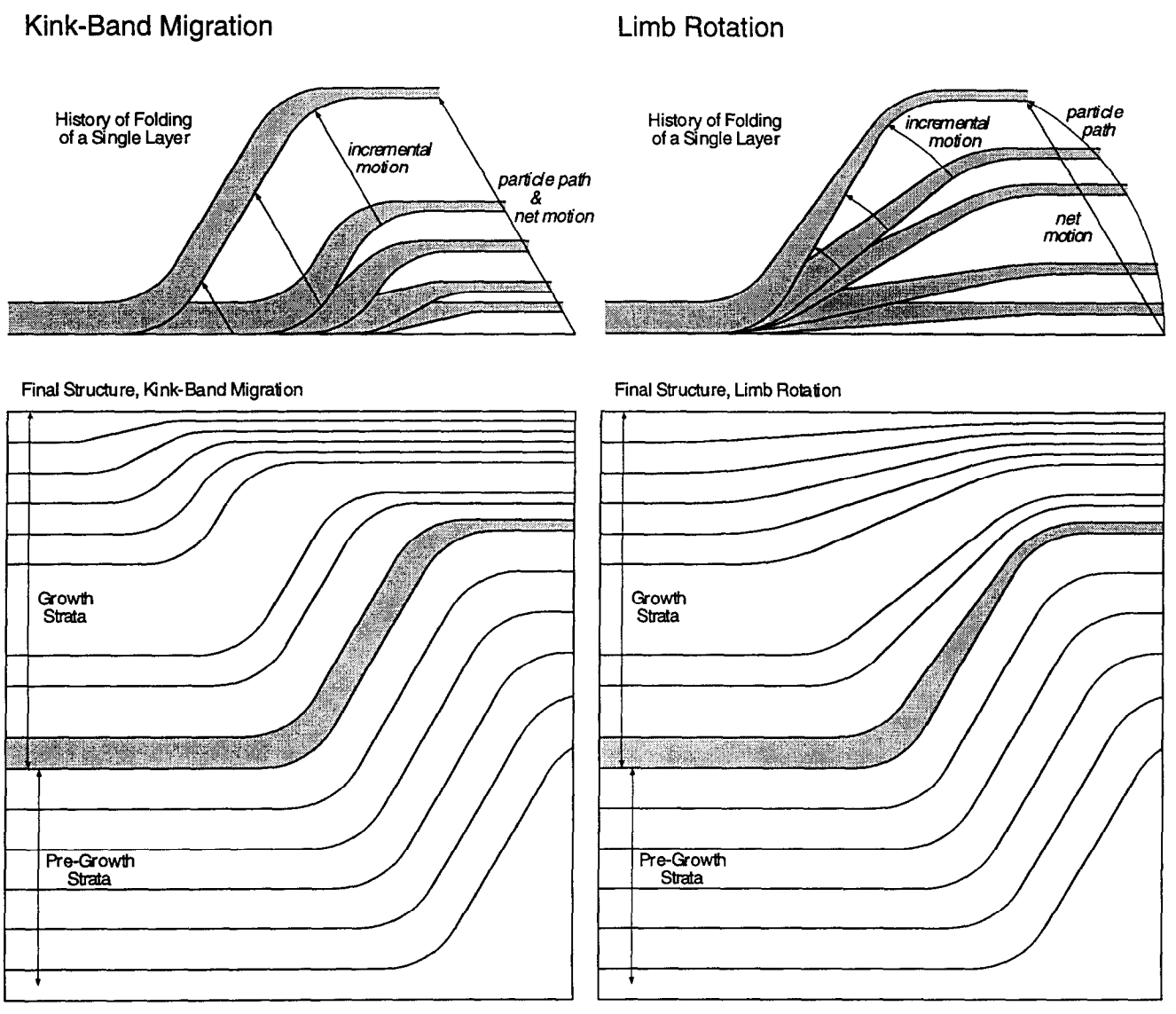

Fig. 1. Balanced forward models of rigid-limb rotation and kink-band migration. The two cross-sections have identical final shapes in the pre-growth strata and have identical stratigraphy. They only differ in the shape of the growth strata in the fold limb, which shows that they have very different kinematic histories.

kinematic behavior of fold hinges that are wide relative to the thickness of mappable beds.

In this paper we analyze the final stages of growth of a major fold near Sant Llorenç de Morunys in the eastern Pyrenees of Spain which we have mapped in sufficiently fine detail (1:5000) to begin to resolve the phenomena of fold growth at close to the bed-by-bed scale. Growth strata are exceptionally well exposed on the south flank of the Sant Llorenç fold and completely record the last few hundred meters of fold growth in a several kilometer wide fold limb.

Contrasting models of fold growth

Sant Llorenç de Morunys is also of substantial interest because of contrasting concepts of fold kinematics within the structural geology community. This structure is often cited as a classic example of folding by rigid limb rotation, beginning with the pioneer work of Riba (1973, 1976). Although limb rotation may play a role in parts of the larger Sant Llorenç de Morunys structure, we will show that the growth strata require that the final stages of growth are dominated by kink-band migration of the sort that is characteristic of much fault-related folding.

One of the characteristic properties of fault-bend folding is that folds grow by kink-band migration (Suppe, 1983; Suppe *et al.*, 1992). Slip of rock past a fault bend produces a change in bedding dip. The zone of dipping strata widens progressively as more and more rock slips through the fault bend. The model on the left side of Fig. 1 shows the sort of fold geometry that is easily

produced by fault-bend folding; the fold limb has its greatest width in the pre-growth strata and becomes progressively shorter in younger growth strata. Fault-bend fold growth by kink-band migration has been documented in a number of compressional, extensional, and strike-slip examples (Medwedeff, 1989, 1992; Beer *et al.*, 1990; Mount *et al.*, 1990; Suppe *et al.*, 1992; Xiao and Suppe, 1992; Narr and Suppe, 1994; Novoa and Suppe, 1994; Shaw *et al.*, 1994a,b; Shaw and Suppe, 1994, 1996; Zapata and Allmendinger, 1996).

In contrast, folding mechanisms such as buckling predict progressive limb rotation. Also the trishear, displacement-gradient, and some detachment folding models of fault tip-line folding predict limb rotation, whereas box, lift-off and fault-propagation folding models predict kink-band migration (for example Jamison, 1987; Suppe and Medwedeff, 1990; Erslev, 1991; Mosar and Suppe, 1992; Hardy and Poblet, 1994; Epard and Groshong, 1995; Homza and Wallace, 1995; Poblet and Hardy, 1995; Wickham, 1995; Poblet and McClay, 1996). Examples of fold growth by limb rotation include Holl and Anastasio (1993), Poblet and Hardy (1995), Vergés *et al.* (1996) and Zapata and Allmendinger (1996). Furthermore, natural folds of mixed origin are known (Fisher and Anastasio, 1994; Hedlund *et al.*, 1994). Limb rotation can also be produced by more complex forms of fault-bend folding which nevertheless involve kink-band migration; for example, displacement on curved normal

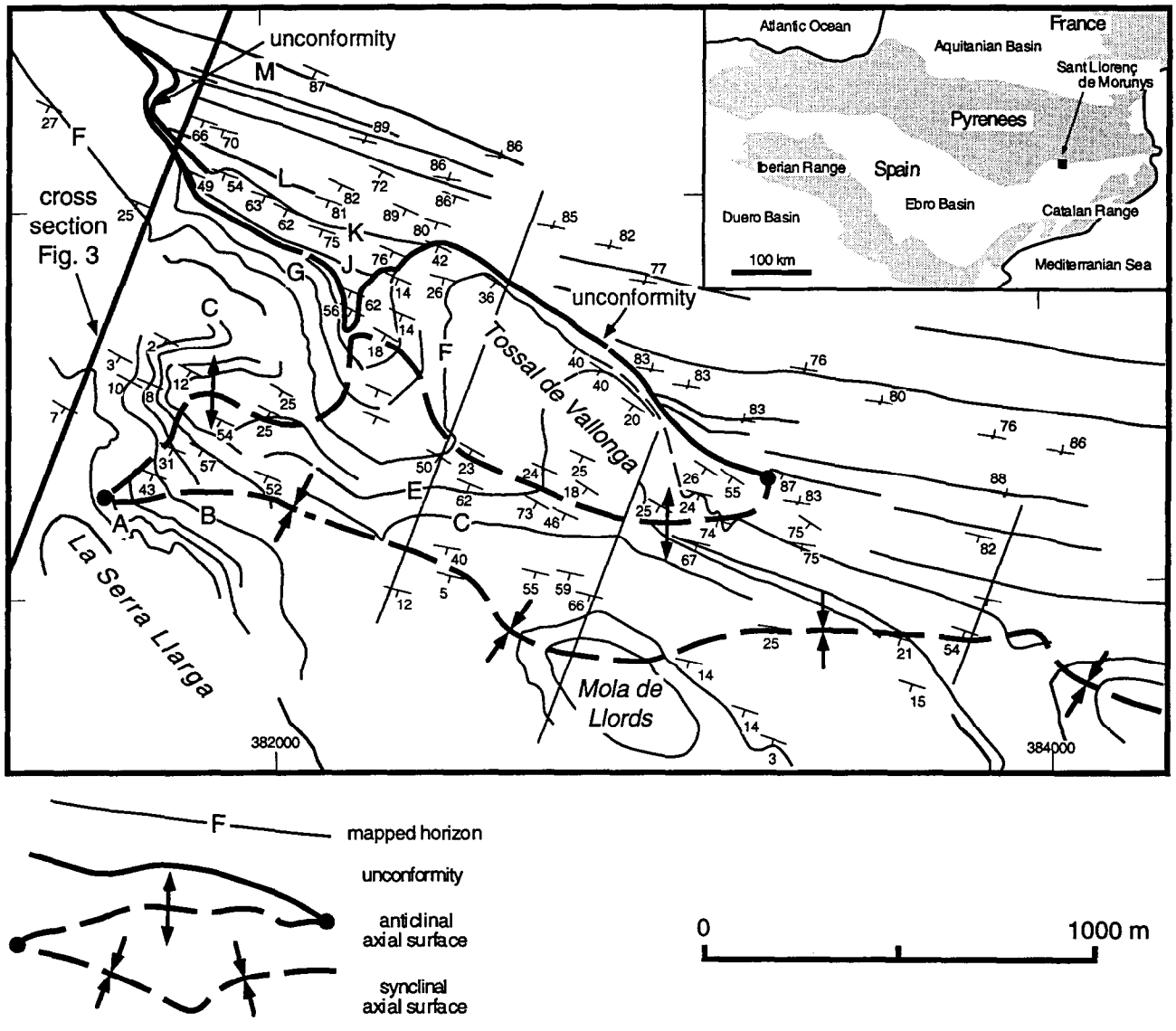

Fig. 2. Simplified geologic map of the Sant Llorenç de Morunys growth structure, eastern Pyrenees, Spain. The synclinal and anticlinal axial surfaces merge to the west, marking the termination of growth. The anticlinal axial surface terminates to the east at the unconformity, reflecting the beginning of the young episode of higher sedimentation rate relative to deformation rate (horizons *I* through *A*). Letters labeling the mapped horizons correspond to the letters of horizons on the cross-section (Fig. 3). Subsidiary cross-sections used in the analysis shown in light lines.

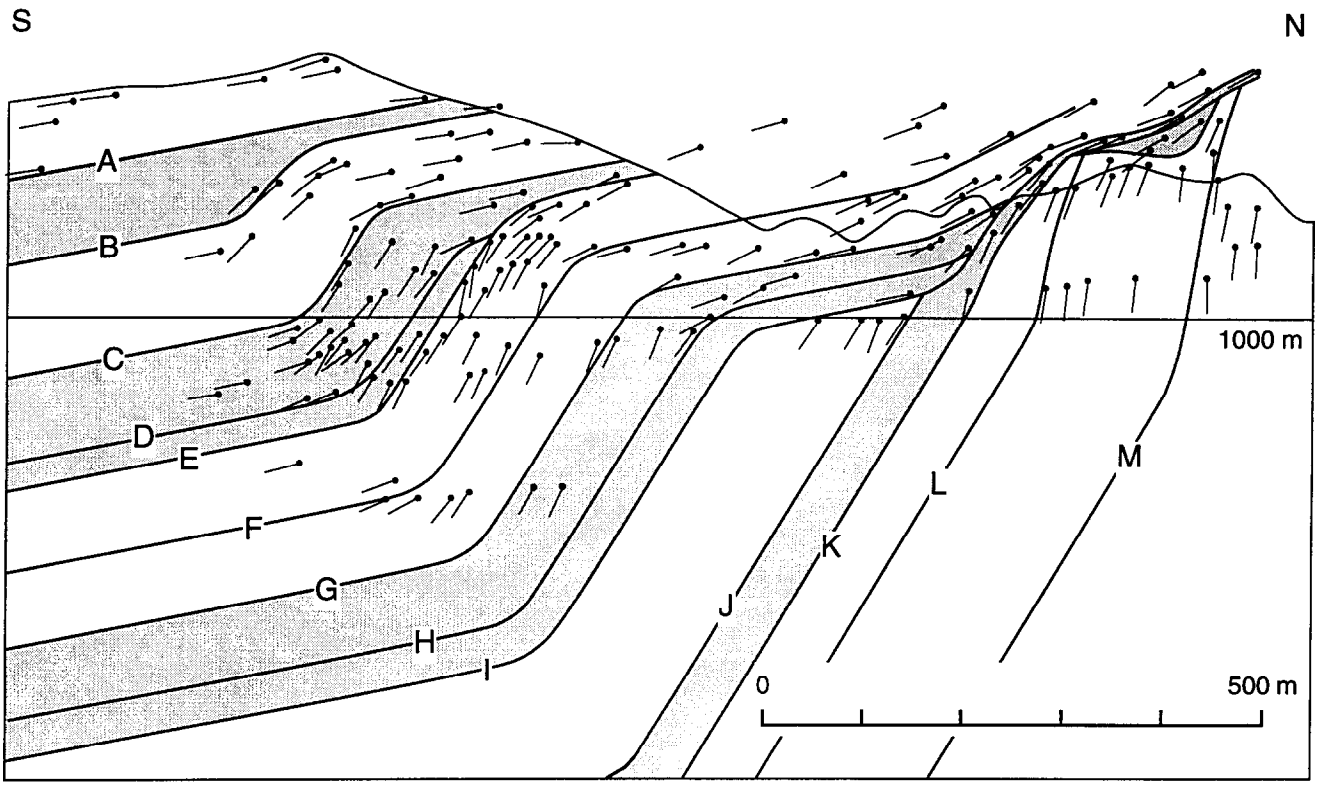

Fig. 3. Geologic cross-section of the Sant Llorenç de Morunys growth structure. The location of the cross-section is shown on the left side of Fig. 2.

and thrust faults produces folds in growth strata showing limb rotation that have been successfully modeled as a convolution of superposed migrating kink-bands (Xiao and Suppe, 1992; Medwedeff and Suppe, 1997). Thus the distinction between the different underlying mechanisms of limb rotation requires some attention to fine details.

Data requirements for deciphering fold growth kinematics from growth strata

The primary geologic data that allows us to decipher the fold kinematics is the progressive sequence of shape and thickness variations of mapped beds within the growth section. Errors in the shape, which can come from mistakes in correlation, map location, topographic base map, and projection into cross-section, will translate directly into errors in the kinematic analysis. Thus, the normally routine tasks of geologic mapping and cross-section construction becomes substantially more demanding when the goal is a detailed understanding of fold kinematics. For example we can no longer necessarily make the routine assumptions of constant layer thickness and cylindrical projection.

Furthermore, it is very difficult or impossible to obtain a qualitatively undistorted understanding of growth structure viewed in mountainous landscape because of the combination of complex intersection of structure with topography, *a priori* unknown thickness variations and distortions from parallax. For example, the photographs of the growth structures at Sant Llorenç de Morunys shown in this paper contain substantial distortion that is not easily evaluated qualitatively; it is difficult to distinguish true thickness variations from apparent thickness variations caused by parallax. It is only by accurate mapping and correct projection of data into cross-section that an undistorted image of the structure emerges.

Thus the study of bed-by-bed growth demands that we be confident that we have an accurate image of the shape of the growth horizons, therefore a brief mention of the

Fig. 4. Photographs of the Sant Llorenç de Morunys growth structure all looking west. The stratigraphic horizons are labled. (a) and (b) show the southern half of the cross-section (Fig. 3) and (c) shows the northern half. (a) The anticlinal growth axial surface viewed from Mola de Llords. The synclinal active axial surface runs up the valley at the far left and merges with the anticlinal hinge just out of view. (b) The anticlinal growth axial surface with the termination of growth marked by the nearly horizontal strata at the top of the cliff (La Serra Larga), viewed from Tossal de Vallonga. The synclinal active axial surface runs up the valley to the left. (c) The growth unconformity viewed from north of Tossal de Vallonga. (d) Anticlinal growth axial surface on the east face of Tossal de Vallonga showing an offset of the anticlinal hinge zone along a disconformity. The anticlinal axial surface terminates at the strong angular unconformity at the base of the cliff face on the right side of Tossal de Vallonga. The active synclinal axial surface runs up the valley to the left and up the cliff face of Mola de Llords to the left.

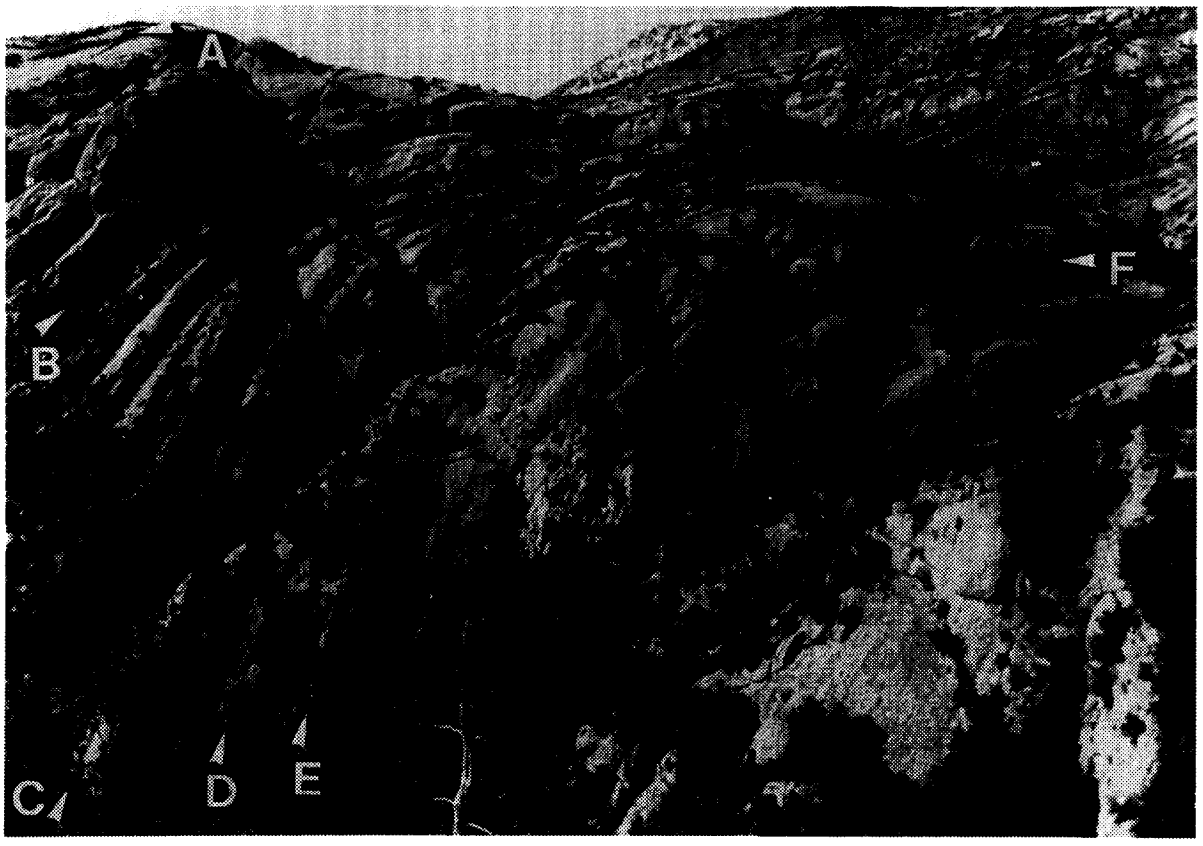

(a)

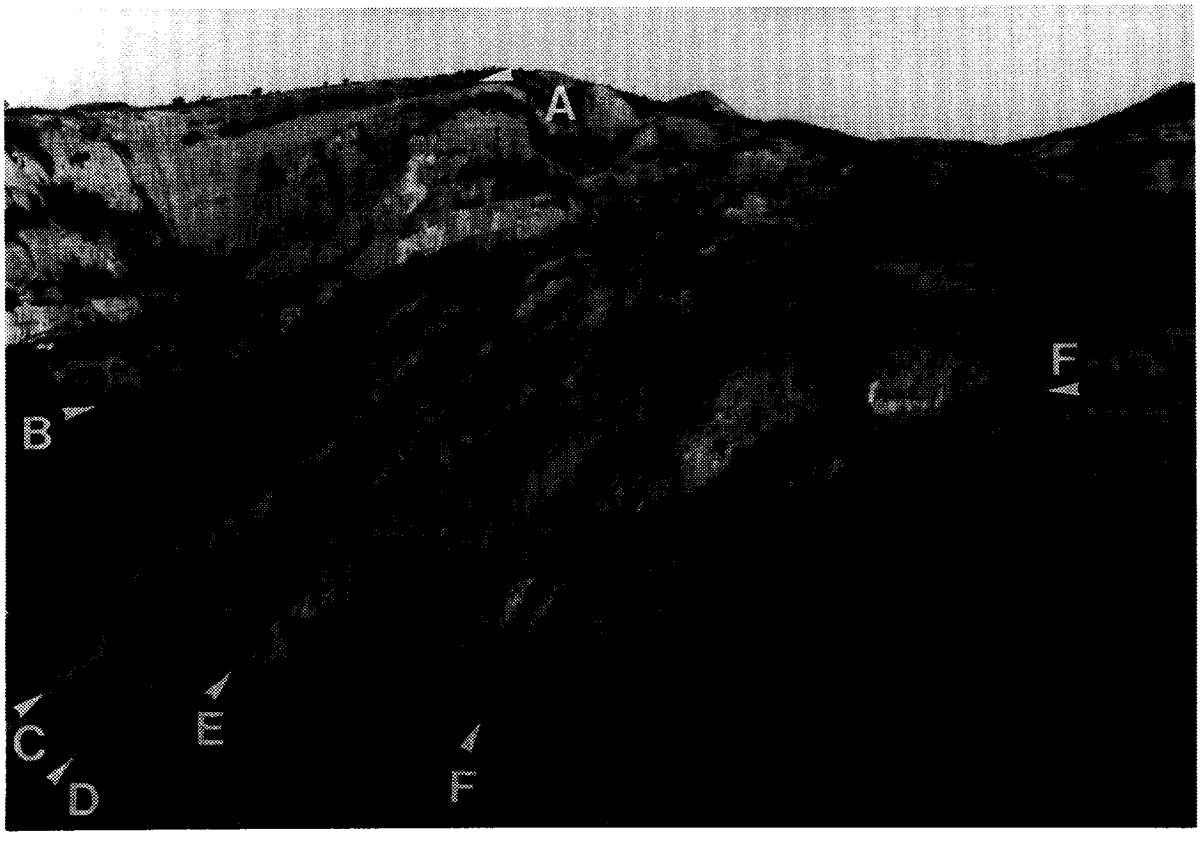

(b)

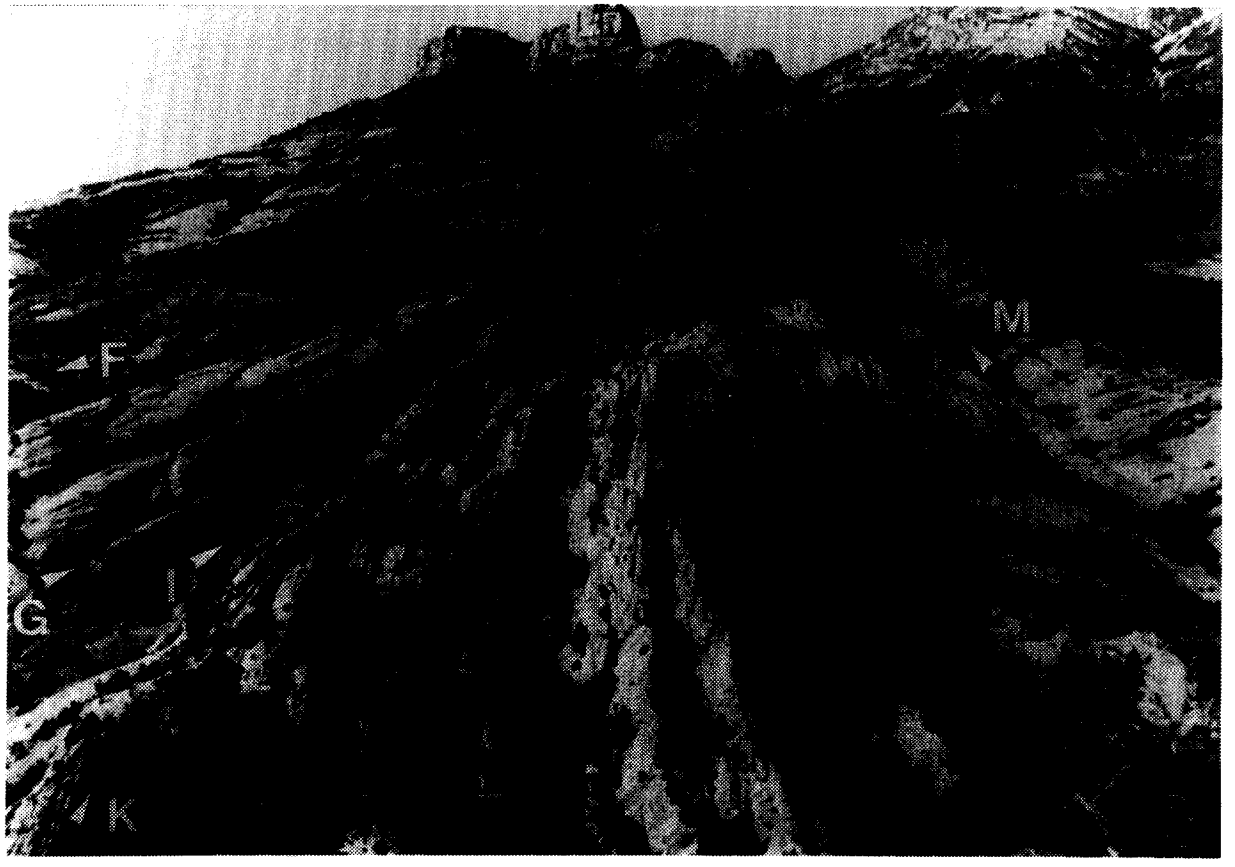

(c)

(d)

methodology of our study of Sant Llorenç de Morunys is appropriate. Sufficiently accurate remapping of this structure became practical in 1994 with the publication by the Cartographic Institute of Catalunya of co-registered orthophotos and topographic maps at a scale of 1:5000 with a contour interval of 5 m. This combination allows accurate location except in areas of cliffs where the topographic map is significantly distorted and correction was required. Special effort was made to correctly trace stratigraphic horizons through the area to obtain the present shapes of specific horizons and to obtain a dense distribution of dip data. A very simplified map is given in Fig. 2.

Stratigraphic and dip data were projected into a composite cross-section using a simple technique of stacking local cross-sections to obtain an undistorted image of the growth structure without producing a full 3-D data model (Fig. 3). The nominal location of the composite cross-section is shown on the geologic map (Fig. 2), as well as the locations of the component local sections. These local cross-sections involved very short distance data projections along locally determined fold axes, which in this case happen to be nearly horizontal and cylindrical; the local sections were then stacked (registered) to obtain the composite section (Fig. 3). This simple technique has the advantage that it preserves the local dispersion in dip data, of which stratigraphic dispersion is the major component, while maintaining the relative positions of the data points. The parts of the fold that are relatively cylindrical can then be stacked or superimposed. Most of the data come from a 600 m wide band in the western half of the area, where strong overturning is absent (Fig. 2).

SANT LLORENÇ DE MORUNYS GROWTH STRUCTURE

Regional setting in the Ebro basin on the south flank of the Pyrenees

Synorogenic strata are widely exposed in the Ebro basin on the southeastern flank of the Pyrenees and provide a remarkable record of compressive deformation from uppermost Cretaceous to lowermost upper Oligocene (approx. 80–25 Ma), with a total shortening of 125–150 km determined from balanced and restored orogen-scale transects (Muñoz, 1992; Vergés *et al.*, 1995). This shortening was accommodated by the thrusting at upper crustal levels and by subduction below the European plate at lower crustal and upper mantle levels, as imaged in the deep reflection ECORS–Pyrenees profile (Choukroune *et al.*, 1989) and magnetotelluric methods (Pous *et al.*, 1995). The Ebro basin is a flexural foreland basin that developed on the down going Iberian plate at the southern margin of the Pyrenees.

In addition, the Ebro basin was constrained on the southeast and south by the coeval Catalan and Iberian ranges, which are basement-involved compressive structures. The Ebro basin was unusually efficient at trapping synorogenic sediments as it became a closed basin from late Eocene to Middle Miocene (Riba *et al.*, 1983). As a result, the mountain fronts were commonly buried by synorogenic sediments and compressive structures preserving growth strata are typical of the margins of the Ebro basin (Riba, 1973, 1976; Anadón *et al.*, 1986), both for the marine and final continental stage (Puigdefàbregas *et al.*, 1986, 1992). These syntectonic sediments have been used extensively to determine the timing and rates of thrusting in the eastern and central southern Pyrenees (Vergés and Martínez, 1988; Burbank *et al.*, 1992b; Vergés, 1993; Vergés and Burbank, 1996); the upper sheets are generally older, defining a forward progression of thrust initiation. However, in addition to this dominant southward progression, good evidence exists for the coeval hindward activity of thrusts during short episodes (Martínez *et al.*, 1988; Vergés and Muñoz, 1990; Burbank *et al.*, 1992a).

The Sant Llorenç de Morunys growth strata constitute an E–W synformal structure with a northern vertical to overturned limb underneath the South Pyrenean frontal thrust. This structure has been interpreted as a southwards displaced original fault-propagation fold (Vergés, 1993). Growth strata constitute a thick late Eocene–early Oligocene sequence of continental conglomerates that overlies a Middle Eocene sequence of marine marls and sandstones (Riba, 1976).

The conglomerates of Sant Llorenç de Morunys were mapped by Riba (1973, 1976) who recognized a fan-like geometry as an important indicator of fold growth during deposition and erosion. This geometry was defined as a *composite progressive unconformity* which according to Riba includes two single progressive unconformities (fan-like wedges) articulated by an angular unconformity, both dominated by lower sedimentation rates relative to uplift rates. The lower one consists of a rotative offlap and integrates the vertical to overturned beds. The upper one consists of a rotative onlap involving south-dipping beds. This study is mainly focused on the growth strata corresponding to the upper progressive unconformity of Riba (1976).

Composite cross-section of growth structure

The cross-section (Fig. 3) shows a structure that is in some ways similar to the model cross-sections of Fig. 1, but more complex in detail. It shows an upward narrowing fold limb with thickness changes concentrated in the anticlinal hinges similar to the kink-band migration model. However, it also shows a decrease in limb dip from 90° in the north to 60° or even 45° in the south which may be suggestive of limb-rotation models. Therefore we need to examine the structure in some detail. Furthermore there is a regional south dip of about 10–15° which is the north limb of the major Serra de Busa syncline (Riba, 1976); this is a younger structure and therefore

represents a refolding of the growth structure that is the concern of this paper.

This cross-section can be separated into two regions characterized by different rates of sedimentation relative to deformation: (1) the northern part which is dominated by angular disconformities (Suppe *et al.*, 1992) or angular unconformities within the growth section (Fig. 4c) and (2) the southern part which is characterized by relatively higher deposition relative to deformation and records the termination of growth (Fig. 4a & b).

The structure is dominated by a 60° south-dipping limb, bounded on the south by a synclinal axial surface that bisects the two fold limbs. Therefore stratigraphic thicknesses do not change significantly across the syncline. In contrast the anticlinal axial surface on the whole does not bisect the two limbs, because the overall stratigraphic thickness of the anticlinal crest is 40–50% less than in the limb. The change in thickness for each mapped interval is localized in the anticlinal hinge, similar to the kink-band migration model of Fig. 1 and in contrast with the limb rotation model, which shows a thickness transition distributed over the entire fold limb. Furthermore the limb dip in the southern half of the cross-section is relatively constant at about 60° within the fold limb away from the curved fold hinges. Finally the limb length between the anticline and syncline decreases stratigraphically upward until the fold limb disappears 50–60 m below the top of the mountain, also consistent with the kink-band migration model. This upward disappearance of the fold limb can be seen in the photographs of Fig. 4(a & b).

However, the anticlinal axial surface is more complex in detail. Some stratigraphic intervals show substantial changes in thickness across the anticlinal hinge, especially the intervals between horizons *A–B*, *C–D*, *D–E*, and *G–H*. In contrast other intervals show little change in thickness, especially intervals *B–C*, *E–F*, and *F–G*, indicating that little deformation took place during those intervals. Either deformation or sedimentation or both have not been constant during growth of the Sant Llorenç de Morunys structure.

The northern part of the cross-section is dominated by several unconformities (Fig. 4c) that are closely linked to the anticlinal axial surface. The anticlinal axial surface terminates at the end of an angular unconformity at the base of horizon *I* which cuts out all of the strata between horizons *I* and *J*. This unconformity appears to be at the regional dip and parallel to overlying strata in the south and quickly turns to be a buttress unconformity just below horizon *J*, with the interval *I–G* terminating against paleotopography to the north (another smaller buttress disconformity terminates the *E–D* interval). Below this buttress unconformity bed *J–K* is progressively thinned up dip because of erosion, but then abruptly bends through an anticlinal hinge to the regional south dip. Note that the anticlinal hinge of interval *J–K* terminates at unconformities above and below. The downward termination of the hinge is at horizon *K* at the end of a strong angular unconformity similar to the termination of anticlinal hinge in the south at horizon *I*. To the north of the hinge a channel appears at the base of the unconformity. To the south of the hinge a slight angular unconformity exits for about 100 m down-dip at the base of horizon *K*. Also, the beds of the

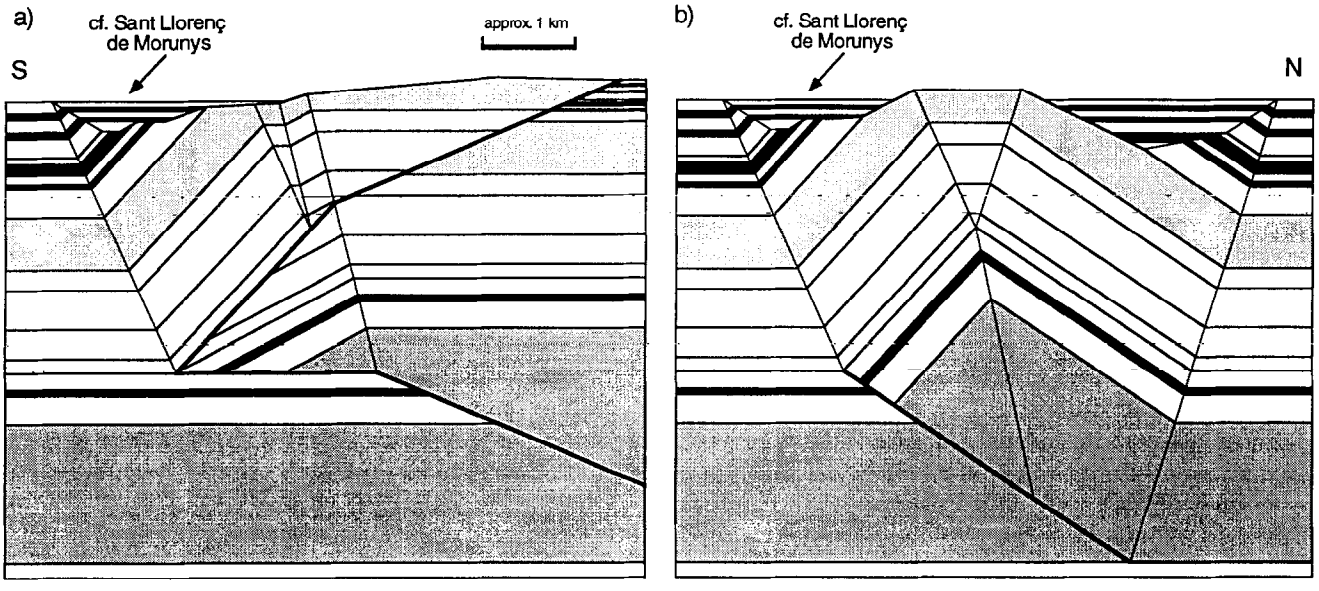

Fig. 5. South-vergent wedge and fault-propagation fold models producing south-limb growth structure similar to that of Sant Llorenç de Morunys. The limb width and fault depth can be varied substantially without effecting the geometry of the final stages of growth on the south limb. These models do not attempt to illustrate the refolding present at Sant Llorenç de Morunys.

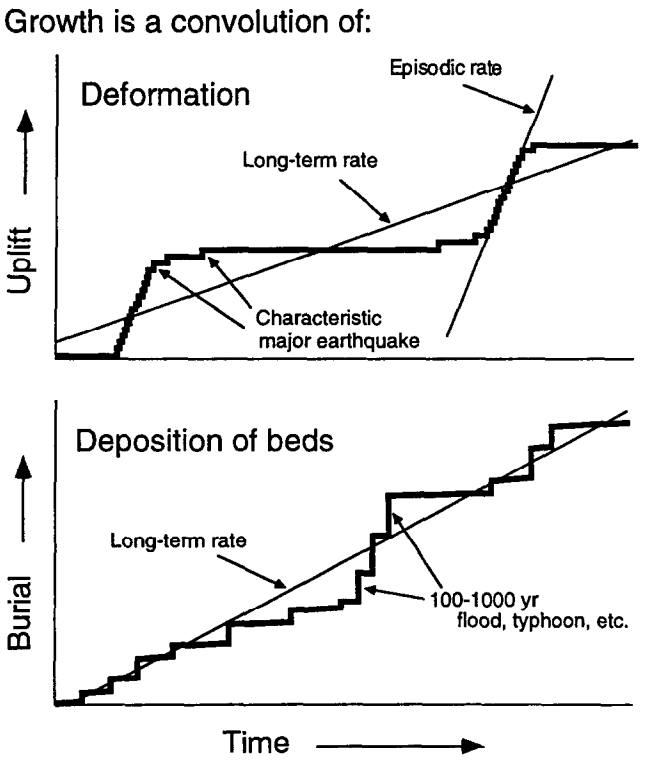

Fig. 6. The detailed shape of a growth structure at various length scales is controlled by the convolution of deformational and depositional events, both of which can be geologically instantaneous or steady. This schematic figure emphasizes the possibility of sudden events and episodes at several timescales: (i) characteristic earthquakes and storms on a 100–1000 year timescale and (ii) climatic and mechanical variations on 10,000–100,000 year timescale.

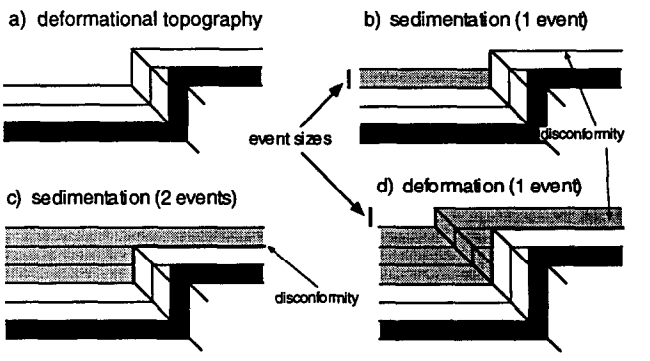

Fig. 7. Fold growth is here modeled schematically as a convolution of sudden quantum deformational and depositional events. The deformational topography of (a) and (d) is preceded by deformational events that cause topography to rise above the depositional surface. Sedimentation events in (b) and (c) buttress against and bury this topography. The segmentation of the anticlinal growth axial surface results in this model from the fact that deformation and sedimentation are sudden or episodic events that are independent or out of phase and because deformation is by kink-band migration.

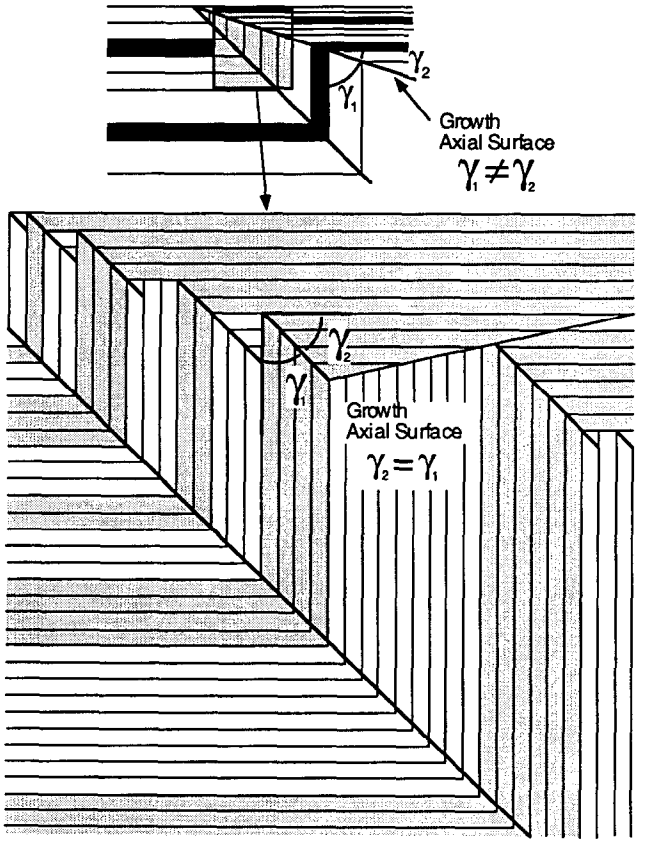

Fig. 8. Schematic model of a growth structure at the bed-by-bed scale. At a scale of kilometers (top), the growth axial surface does not bisect the anticlinal hinge because there is a thickness change across the fold. In contrast, at the bed scale of our simple quantum model (Fig. 7), the growth axial surface fragments into a number of bisecting axial surfaces linked by disconformities and unconformities. In this model, individual beds do not change thickness, therefore the axial surfaces bisect. The larger-scale change in thickness across the fold is accomplished by bed loss, through buttressing against paleo-topography and erosion.

K–M interval have a lower dip directly below the unconformity but show no important down-dip variation in thickness of the sort that would be predicted by limb-rotation models. We will attempt to explain all these fine details of the structure with our theory of bed-by-bed growth.

Riba (1973, 1976) interpreted the progressive changes in dip from north to south as suggestive of progressive limb rotation. However, the basic structural concepts of fold growth above moving thrust faults were not well developed in the 1970s when Riba did his pioneering work, nor were detailed maps available (his work is an excellent example of combined airphoto and field analysis). Therefore he was not able to fully confront the details of the deformation; rather he emphasized the basic insight that these were a set of progressive growth unconformities. More recent study of fold growth above thrust sheets shows that such peculiar unconformities linked by anticlinal hinges are characteristic of folding by kink-band migration (Suppe and Medwedeff, 1990; Suppe *et al.*, 1992). Furthermore, Riba's cross-section correctly shows the upward narrowing fold limb to the south; more recent studies show that such growth triangles are easily explained by kink-band migration (Suppe and Medwedeff, 1990; Suppe *et al.*, 1992; Shaw and Suppe, 1994, 1996), although they could also be

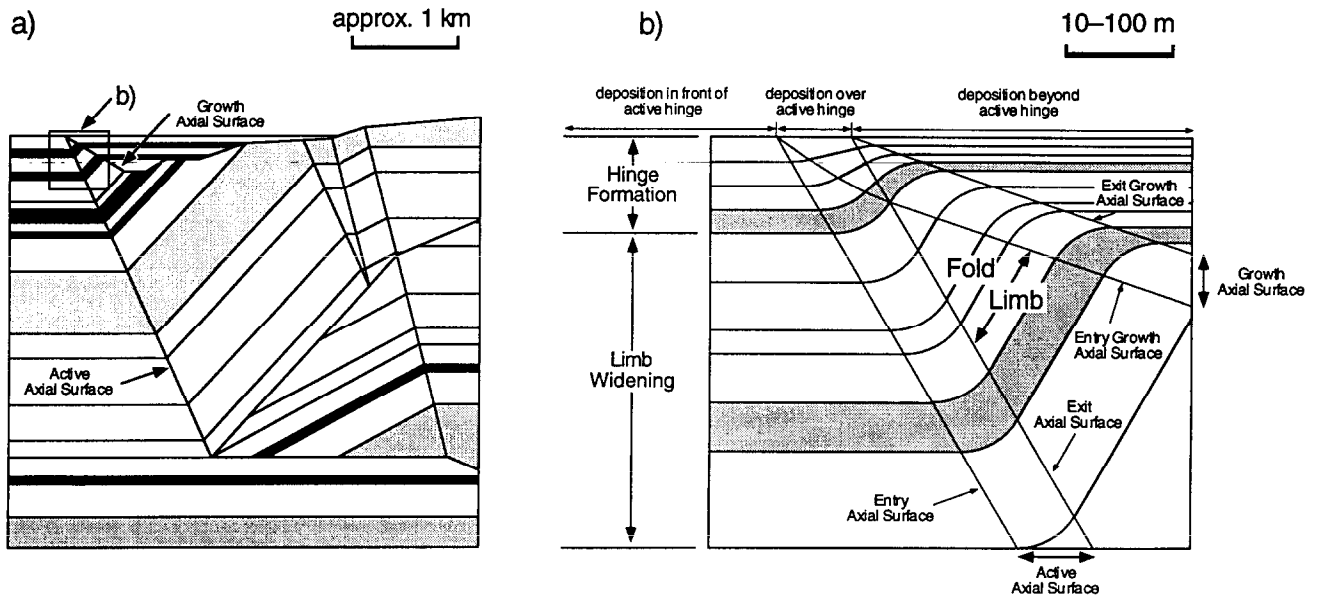

Fig. 9. Understanding curved-hinge kink-band migration requires expanding the sharp axial surface lines of models such as (a) to become a zone of finite width, as in (b), bounded by *entry* and *exit axial surfaces*. Similarly, the point at which the growth axial surface and active axial surface meet at a large scale (a) expands to be a zone of finite thickness in (b), the zone of progressive hinge formation. Particles that are deposited over the active hinge zone undergo different kinematic histories to particles deposited to either the left or right, as shown in Fig. 10.

explained by a combination of limb rotation and kink-band migration (Poblet *et al.*, 1997), with the finer details of the shape distinguishing these possibilities.

We now attempt to understand the growth of the Sant Llorenç de Morunys structure at the scale of our new mapping, making use of balanced forward modeling and restoration.

BED-BY-BED FOLD GROWTH: FORWARD MODELING

Plausible simple fault-related fold models

The last stages of growth of the Sant Llorenç de Morunys structure, which is the emphasis of this paper, shows a number of features indicative of folding by kink-band migration, as touched on above. Observations that may suggest folding by limb rotation are the southward decrease in limb dip and down-dip thickening, largely in the intervals *A–C* and *J–L*. The decrease in dip in the *A–C* interval is interpreted below as an effect of the processes of near-surface hinge-formation at the final stages of growth. The decrease in dip in interval *J–L* is explained in our cross-section by multiple refolding and kink-band interference (Novoa and Suppe, 1994; Medwedeff and Suppe, 1997), but is beyond our scope. The down-dip thickening can be explained by omission and erosion of beds between unconformities as in the interval *K–L* (Fig. 3). In this subsection we simply show that there are several types of fault-related folding capable of satisfying the last stages of growth of the Sant Llorenç structure, without specifically modeling the structure (Fig. 5).

Figure 5 shows two simple balanced forward models involving south-vergent thrusting, both producing a growth triangle on their south flank similar to Sant Llorenç with an active synclinal axial surface and the same front-limb dip (59°, similar to Sant Llorenç before refolding). It should be emphasized that the width of the front limb is fully adjustable in both models of Fig. 5 and that the near-vertical and overturned dips of the actual structure as well as the regional south dip can be modeled by refolding by fault-bend folding. In the context of this paper we only wish to indicate two plausible origins of the kink-band migration before we move to a much higher-resolution analysis of the growth strata.

Figure 5(a) is a south-vergent wedge model with the two thrust ramps dipping symmetrically at 23°, essentially at the Coulomb-fracture angle. This model is closely similar to the Wheeler Ridge anticline in California studied by Medwedeff (Medwedeff, 1992; see also Mueller and Suppe, 1997), which is very well constrained by numerous boreholes; thus we have a well documented structural analog for this model.

Figure 5(b) is a south-vergent fault-propagation fold model with a ramp angle of 34° and a front-limb dip of 59°. This model is closely similar to a structural solution given by Suppe and Medwedeff (1990) for the Puli anticline in Papua New Guinea, partially constrained by surface and borehole data. Thus we have a reasonably good structural analog for this model.

Therefore we have several plausible fault-related folding models for the formation of final stages of

growth of the Sant Llorenç de Morunys structure containing the essential features of a synclinal active axial-surface on the south flank. Distinguishing between these and other models of course requires a much more regional analysis, including a deep cross-section, which is beyond our present scope.

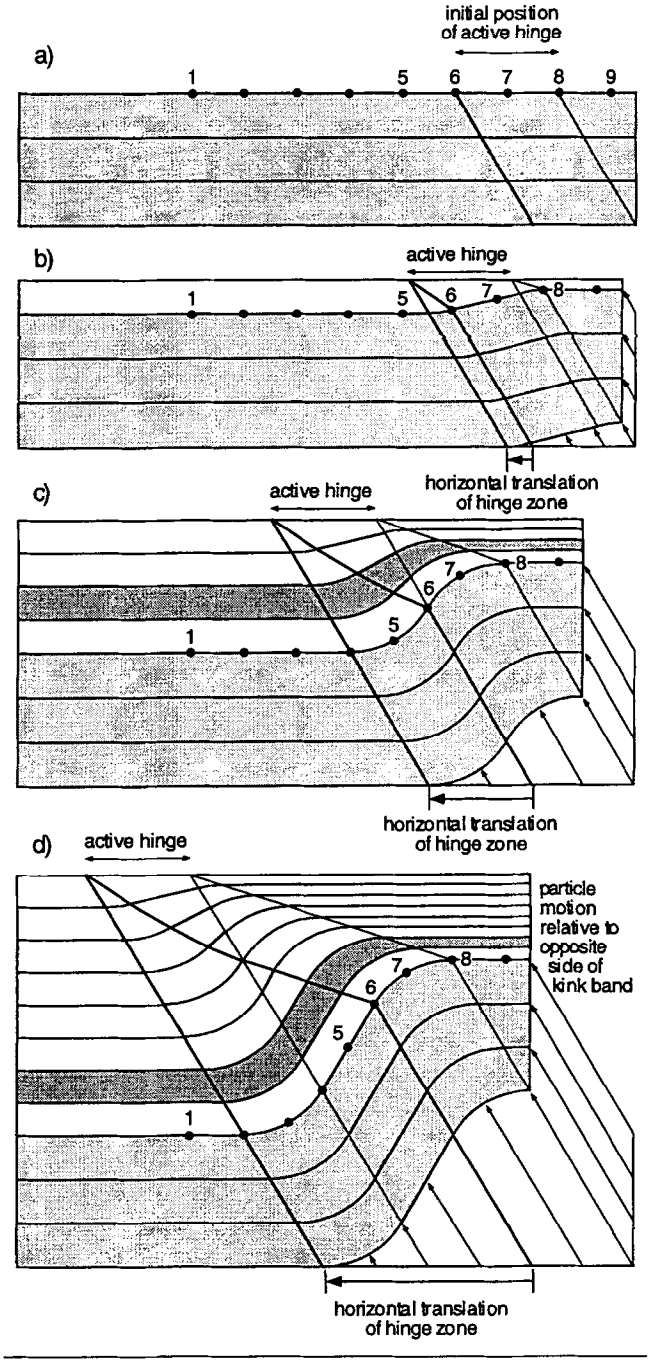

Fig. 10. Model of the sequential development of curved-hinge kink-band migration, in which folding takes place progressively as particles move through the active hinge zone. (a) Particles 6–8 are deposited over the actively deforming hinge zone. (b) As deformation continues particle 8 immediately exits the active hinge zone and translates with the same velocity as particle 9, which was deposited beyond the active hinge zone. (c) Particle 6 is just exiting the zone of active deformation. The anticlinal hinge bounded by particles 6 and 8 is fully formed and no longer changes shape. (d) With continued deformation beyond this stage, particles 1–5 deposited in front of the active hinge will occupy the fold limb.

Forward models of kink-band migration at the bed-by-bed scale

The simple models of fold growth in Fig. 1 are designed to illustrate the basic fold kinematics and therefore have a steady sedimentation rate relative to deformation rate. However, we expect that in many tectonic environments the rates of both deformation and sedimentation can be highly variable. The resulting growth geometry on a bed-by-bed scale will be a convolution of the fluctuations in sedimentation and deformation. Fold growth in many upper crustal structures may grow by fault slip of 1–10 m in large earthquakes (Mueller and Suppe, 1997) separated by hundreds or thousands of years and are possibly grouped by longer time-scale clustering of earthquakes into episodes of deformation and non-deformation (Fig. 6a). Thus, much fold growth may occur in essentially instantaneous events on the order of 1–10 m. In other tectonic environments, deformation may occur as the sum of many smaller earthquakes as well as by aseismic creep, which could be steady state or separated into episodes relative to the timescales of sedimentation.

Bed formation may be quasi-steady state relative to the timescales of deformation, but in many cases bed formation may be catastrophic, for example forming in 100–1000 year floods and typhoons (Fig. 6b). Furthermore, sedimentation shows longer timescale variation controlled by climatic variation.

For environments where we expect sudden deformation and bed formation, we can imagine fold growth by kink-band migration occurring as a convolution of instantaneous sedimentation and deformation events, with little happening in between, as shown schematically in Fig. 7. Thus at some stages (Fig. 7a & d) deformation gets ahead of sedimentation and at other stages sedimentation is catching up or getting ahead of deformation (Fig. 7b & c). The effect of this process over many sedimentation and deformation events, plus times of erosion, is shown in Fig. 8. At a large scale (top of Fig. 8), the growth axial surface does not bisect because there is a thickness change across the fold. In contrast, at the bed-by-bed scale of our simple quantum model (bottom of Fig. 8), the growth axial surface fragments into a number of bisecting axial surfaces linked by disconformities and angular unconformities. In this quantum model individual beds do not change thickness, therefore the axial surfaces bisect. The larger-scale change in thickness across the fold is accomplished by bed loss, by buttressing against topography (Fig. 7b) and by erosion (Fig. 8). This quantum model includes many of the essential features of the Sant Llorenç structure, but it is necessary to consider the effects of finite hinge width because our fold hinges are wide relative to the thickness between our mapped horizons.

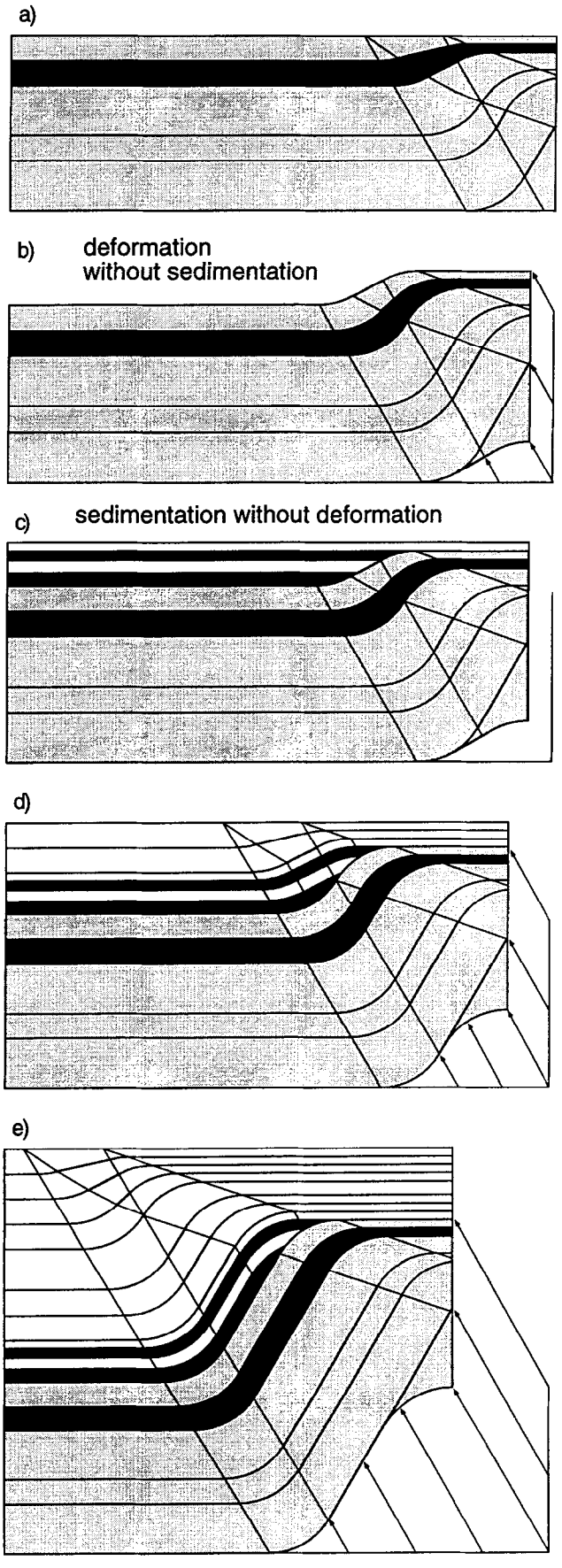

Forward models of curved-hinge fold growth by kink-band migration

Large-scale fault-related folding models such as those of Fig. 5 seek to provide insight into the first-order relationships between fault shape and fold shape. For this reason straight faults and angular fold hinges are appropriate for many structures, although folds produced by curved faults may be modeled with the same techniques (see Xiao and Suppe, 1992; Medwedeff and Suppe, 1997). The key observation is that many large structures have fold hinges which are very narrow relative to limb widths and limb dips are relatively constant over large regions. However, such angular fold models are inappropriate if we wish to fully understand growth structure at the scale of our mapping of the Sant Llorenç structure, which begins to resolve the details of hinge-zone shapes. Therefore we need a balanced forward model of growth folding by kink-band migration that incorporates curved hinges that are wide relative to layer thickness.

The essential task of modeling curved-hinge kink-band migration is to expand the sharp axial surfaces of models, such as Fig. 9(a), to have a substantial width, such as in Fig. 9(b). It is sufficient for the purposes of this paper to model these wide axial-surface zones as curved similar folds; the fact that layer thickness and bed length are not conserved within the hinge zone is not important for the phenomena we seek to model. The axial-surface line at a large scale in Fig. 9(a) expands to be a zone of finite width in Fig. 9(b), bounded by entry and exit axial surfaces. Furthermore, the point at which the growth axial surface and active axial surface meet at a large scale in Fig. 9(a) expands to be a zone of finite thickness in Fig. 9(b) (the zone of hinge formation).

It may take 10–100 major earthquakes over a period of perhaps 1000–100,000 years for particles to traverse a 10–100 m wide hinge zone and be fully folded (Fig. 9b). Thus in our curved-hinge model (Figs 9b & 10) a bed just deposited is composed of three parts: (1) particles deposited over the actively folding hinge zone, (2) particles deposited in front of the active hinge zone, such that they will enter the active hinge zone as deformation continues and (3) particles deposited beyond the active hinge zone, such that they will never enter the active hinge zone. For example in Fig. 10(a), particles 6–8 are deposited over the actively deforming hinge zone. As deformation continues to the stage of Fig. 10(b), particle 8 immediately exits the active hinge zone and undergoes rigid-body translation with the same

Fig. 11. An otherwise steady-state curved-hinge growth model showing a perturbation consisting of (b) deformation without sedimentation, followed by (c) sedimentation without deformation, followed by a resumption of steady-state growth. Once this perturbation exits the active hinge zone (e), we see the deformation without sedimentation as an offset in the anticlinal growth hinge along a disconformity and the sedimentation without deformation as a bisecting of the fold hinge.

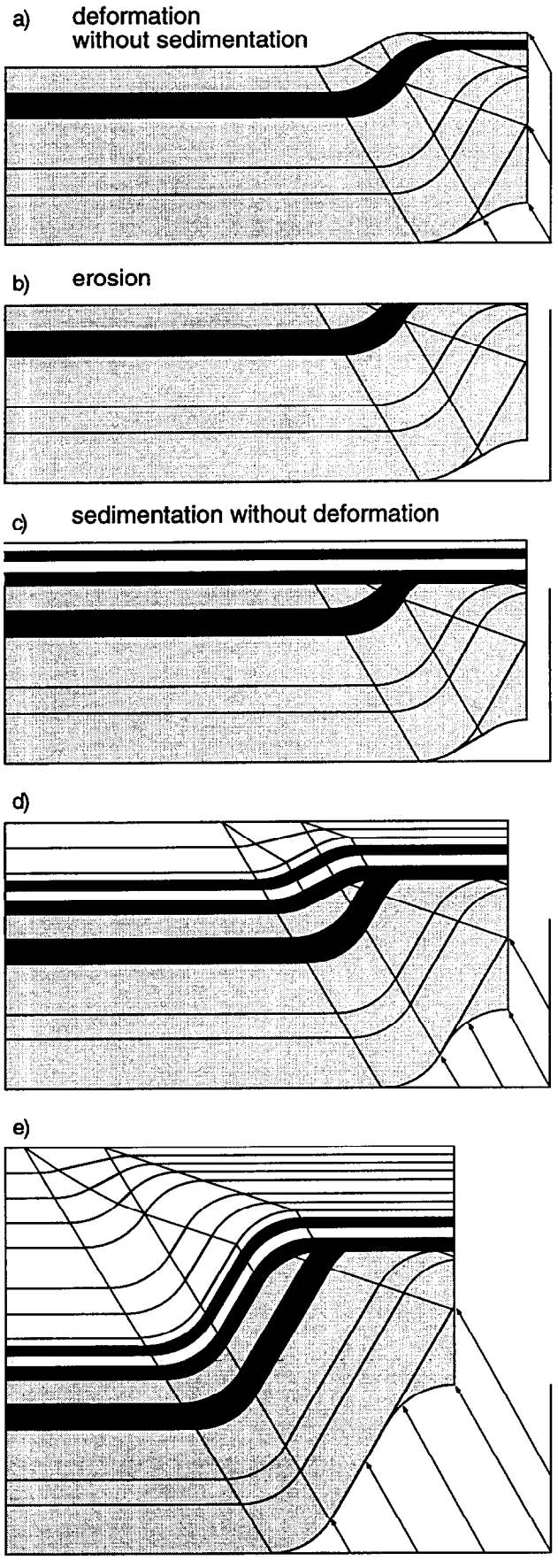

Fig. 12. The same steady-state curved-hinge growth model as Fig. 11, but with the addition of erosion.

velocity as particle 9, which was deposited beyond the active hinge zone. At the stage of Fig. 10(c), particle 6 is just exiting the zone of active deformation and the anticlinal hinge bounded by particles 6 and 8 is fully formed and no longer changes shape (see Fig. 10d). The labeled horizon has exited the zone of hinge formation (Fig. 9b) and enters the zone of limb widening; at this point the particles deposited to the left of the active hinge zone, such as particle 5, begin to exit the active hinge zone and enter the fold limb. With continued deformation beyond the stage of Fig. 10(d) all the particles 1–5 will eventually occupy the fold limb. Thus the fold limb is composed of particles that were deposited in front of the active hinge zone, the anticlinal hinge is composed of particles deposited over the active hinge zone, and the fold crest is composed of particles deposited beyond the active hinge zone.

There is a gradual rotation within the active hinge and a progressive development of the anticlinal growth hinge (Fig. 10). After the anticlinal hinge is fully formed, particles 6, 7 and 8 that were deposited over the active hinge, have traversed progressively less of the zone of active folding, therefore they have progressively lower dips. Particle 8 has a zero dip because it was deposited on the exit axial surface, whereas particle 6 has the dip of the fold limb because it was deposited on the entry axial surface. Thus, particles 5 and 6 have the same dip in Fig. 10(d) because they both moved entirely through the active hinge zone. The entry and exit growth axial surfaces define the locus of all particles deposited over the active hinge zone (Fig. 9b).

Perturbations in the curved-hinge growth model

We briefly introduce the effects of fluctuations in sedimentation and deformation on the curved-hinge growth model (Figs 11 & 12). By analogy with our previous discussion of growth events (Fig. 7), Fig. 11 shows an otherwise steady-state curved-hinge growth model with a perturbation consisting of (1) deformation without sedimentation (Fig. 11b), followed by (2) sedimentation without deformation (Fig. 11c), followed by a resumption of steady-state growth. Once this perturbation exits the active hinge zone (Fig. 11e), we see (1) the deformation without sedimentation as an offset in the anticlinal growth hinge along a disconformity and (2) the sedimentation without deformation as a bisecting fold hinge. The same model with the addition of erosion is shown in Fig. 12. In this case an incomplete fold hinge is seen below the unconformity (Fig. 12e).

Application of forward modeling to Sant Llorenç de Morunys

We can now interpret our Sant Llorenç de Morunys cross-section by comparison with our balanced forward models (Fig. 13). First we are able to define a system of entry and exit active axial surfaces and growth axial

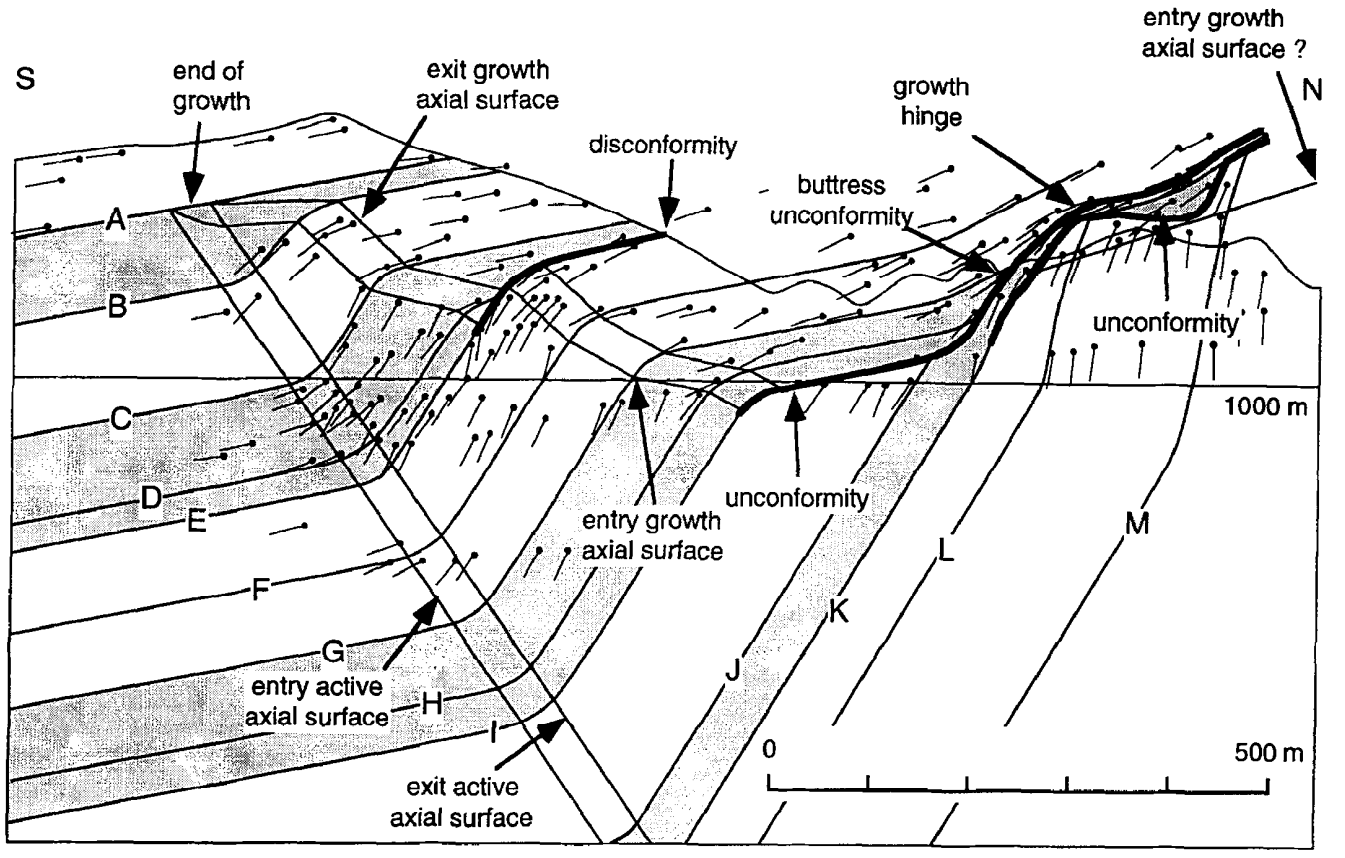

Fig. 13. Sant Llorenç cross-section with the details of the hinge-zones, unconformities, and disconformities interpreted in light of the balanced forward models.

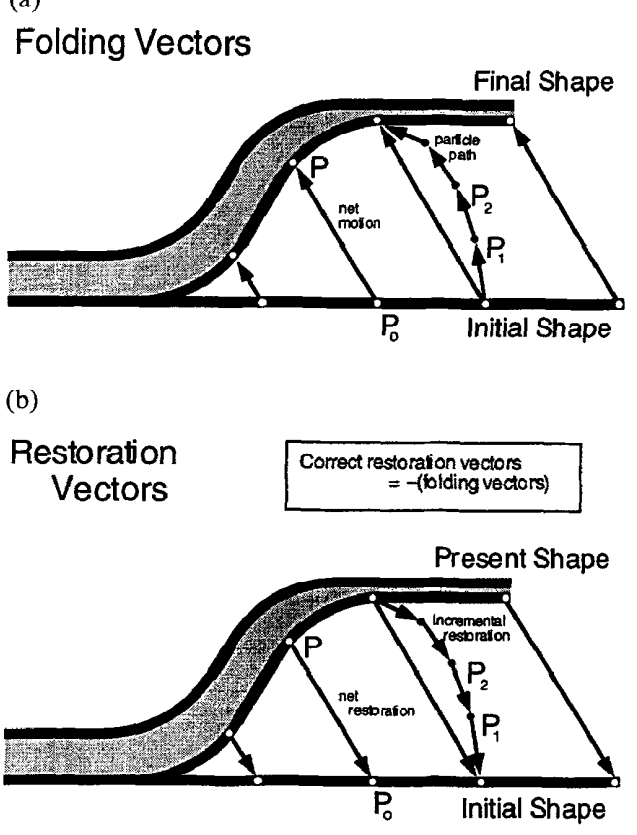

Fig. 14. (a) The net and progressive particle motions of deformation can be described by a field of folding vectors. (b) Restoration, if perfectly done, involves choosing net and incremental restoration vectors that are the reverse of the actual folding vectors.

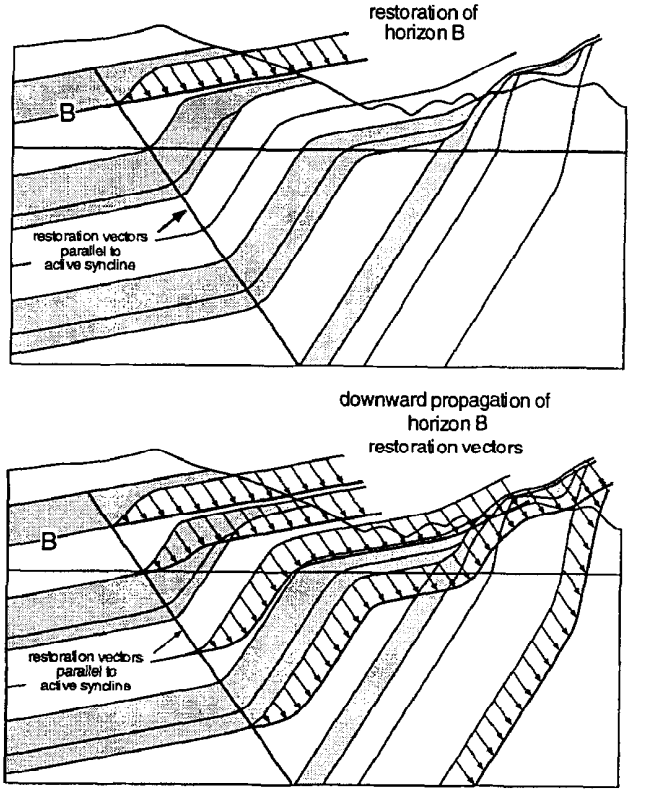

Fig. 15. Restoration of the *B* horizon and downward propagation of the horizon-*B* restoration vectors to subsurface horizons. Restoration vectors are chosen parallel to the synclinal axial surface because that is the orientation that conserves layer thickness and unfolds the syncline properly.

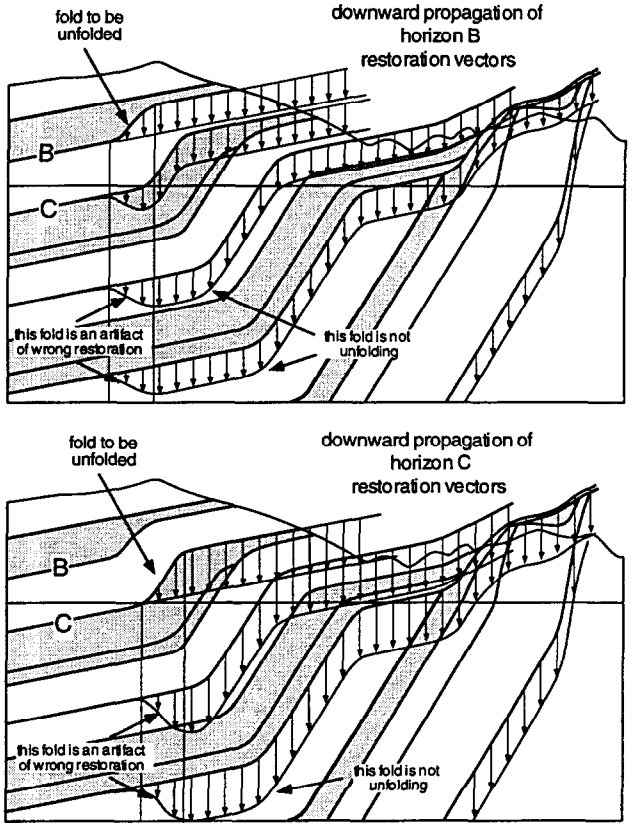

Fig. 16. An example of an incorrect choice of restoration vectors leading to obvious inconsistencies.

surfaces (Fig. 9b) analogous to the curved-hinge models (Figs 11 & 12) and the angular model (Fig. 8). There are offsets in the anticlinal hinge zones along disconformities (horizon *E*) and unconformities (horizon *I*). A similar offset in anticlinal hinge along a disconformity is shown in the photograph of the east face of Tossal de Vallonga (Fig. 4d).

The stratigraphic resolution of much of the growth structure is limited because much of the section is amalgamated conglomerates with no clear bedding. Therefore, the fine structure of the hinge zones is not easily resolved. Nevertheless, intervals *B–C*, *E–F*, and *F–G* (Fig. 13) display very little thickness change and are similar to the non-deformational interval in the curved-hinge growth models of Figs 11(c) and 12(c). In contrast, at the scale of our cross-section, intervals *A–B*, *C–D*, and *G–H* appear similar to the steady-state parts of those models (Fig. 11b, d & Fig. 12d). Thus we see evidence for substantial variation in the convolution of deformation and sedimentation (Fig. 6).

This variation in deformation relative to sedimentation also appears at a larger scale. Deposition averages about 200% of uplift during the *A–I* interval. Deposition averages 60% of uplift for the *I–J* interval. It is possible that the structure below horizon *K* can be interpreted as a growth hinge below an unconformity similar to Fig. 12, but with the entry growth axial surface nearly parallel to the unconformity (Fig. 13), which would imply deposition close to 100% of uplift for the *K–M* interval. Therefore, the fluctuations in the convolution of deformation and sedimentation at Sant Llorenç de Morunys took place at several different timescales.

BED-BY-BED FOLD GROWTH: RESTORATION

Basic concepts of fold restoration

We now analyze the Sant Llorenç de Morunys growth structure by progressive restoration of the cross-section. The basic concept of restoration is that the historic deformation path and net deformation can be described by folding vectors (Fig. 14a). The correct choice of restoration vectors is precisely the reverse of the folding vectors (Fig. 14b). Choice of restoration vectors is strongly constrained by appropriate balancing constraints and by the requirement that at each step in a progressive restoration the growth structure appears geologically reasonable. In the present compressive case it seems that the appropriate balancing constraints would be conservation of layer thickness and bed length, especially given the observed bisecting synclinal axial surface. This balancing constraint is closely approximated by restoration vectors parallel to the bisecting synclinal axial surface (Fig. 15).

Progressive restoration of growth strata generally involves propagation of restoration vectors downward from the depositional surface (Nunns, 1991). For example in Fig. 15 we see the downward propagation of the horizon *B* restoration vectors. However, if we were to choose different restoration vectors, for example a vertical orientation (Fig. 16), which of course does not conserve layer thickness but is common in seismic interpretation software, we find we get geologically unreasonable restorations with clear artifacts that are transient effects with folding immediately followed by unfolding (compare Fig. 16a & b). The nearly homogeneous downward propagation of the restoration vectors parallel to the active syncline used in our restorations is reasonable given the straight fold limb and bisecting active axial surface. However, propagation of incremental restoration vectors homogeneously downward from the surface may introduce some second-order errors because not all deformation at depth will propagate homogeneously to the surface, as discussed by Nunns (1991). Such errors seem to be negligible in our restorations.

Application of restoration to Sant Llorenç de Morunys

We now restore the Sant Llorenç de Morunys cross-section using restoration vectors that conserve layer thickness, similar to those of Fig. 15. Five stages in the restoration are shown in Fig. 17. Note that we are not

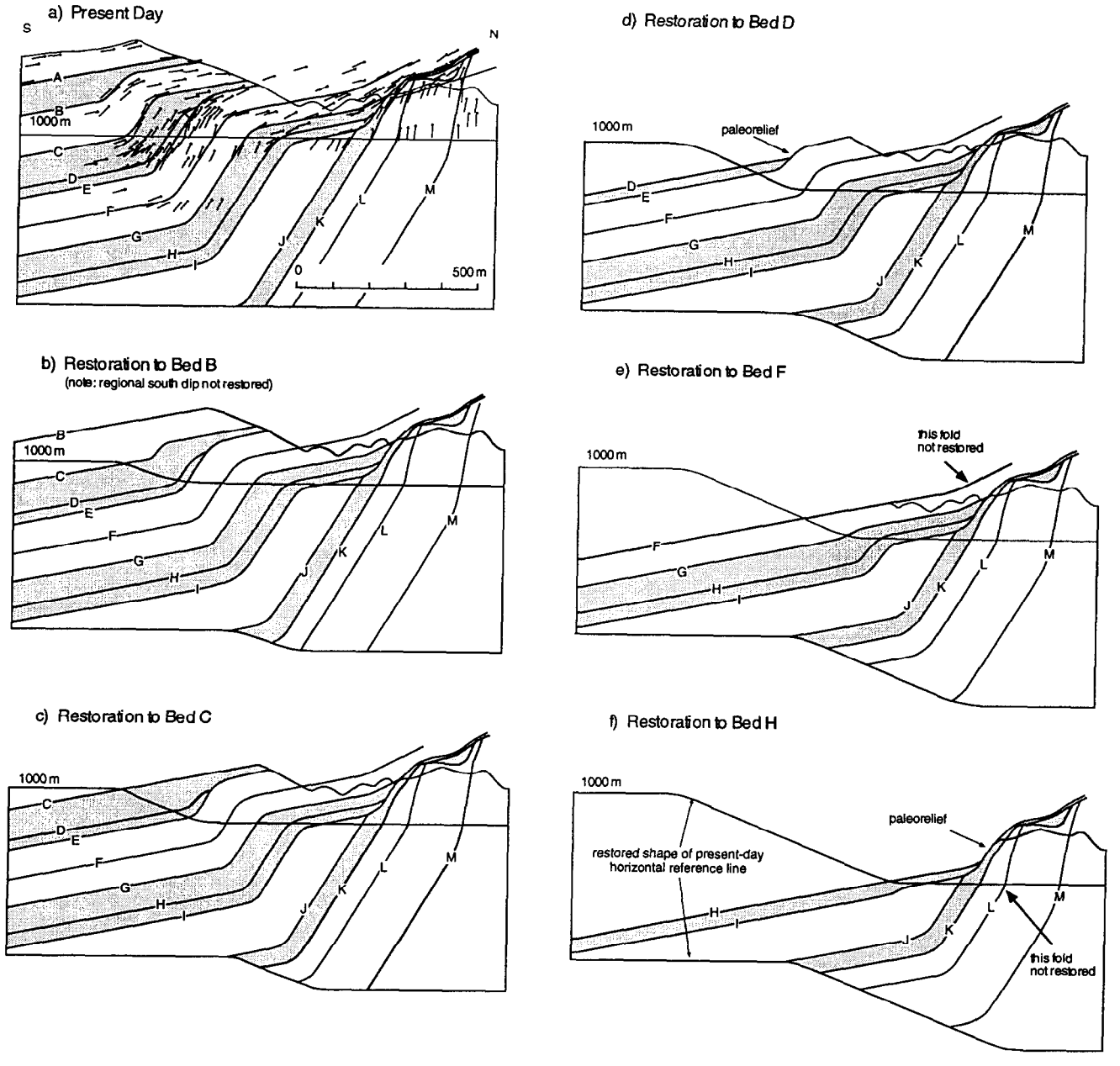

Fig. 17. Sequential restoration of the Sant Llorenç de Morunys using restoration vectors similar to Fig. 15. No attempt is made to restore the younger regional south dip or the refolding in the north (e & f). Note the progressive development of the fold by kink-band migration. The base of the cross-section and 1000 m elevation line in (a) function of passive markers illustrating the kink-band migration.

restoring the younger regional south dip, which would be restored before the horizon *B* restoration (Fig. 17b) or the additional folding of the structure to a steeper dip in the north (Fig. 17e & f); our purpose is to restore the well-constrained growth structure only.

The most important feature of the restorations is that they show a progressive unfolding by kink-band migration. Note also that the active syncline always intersects the depositional surface at the position of the anticlinal hinge for that bed. Significant paleo-relief is present at bed *D* and *H* times (Fig. 17d & f), similar to the forward models (Figs 7 & 11).

The progressive unfolding of the structure by kink-band migration is also shown by the deformation of the 1000 m elevation horizon and the base of the cross-section, which are undeformed markers in the present day cross-section (Fig. 17a). Approximately 300 m of horizontal kink-band migration is shown between bed *H* time and the present.

These restorations also allow us to look at the progressive deformation paths of single beds or horizons, similar to the top of Fig. 1. Figure 18 shows the progressive deformation of horizon *F* and beds *D–E* and *H–I*. In each case an increasing limb length at constant dip through kink-band migration is demonstrated.

It is important to note that our restorations are entirely

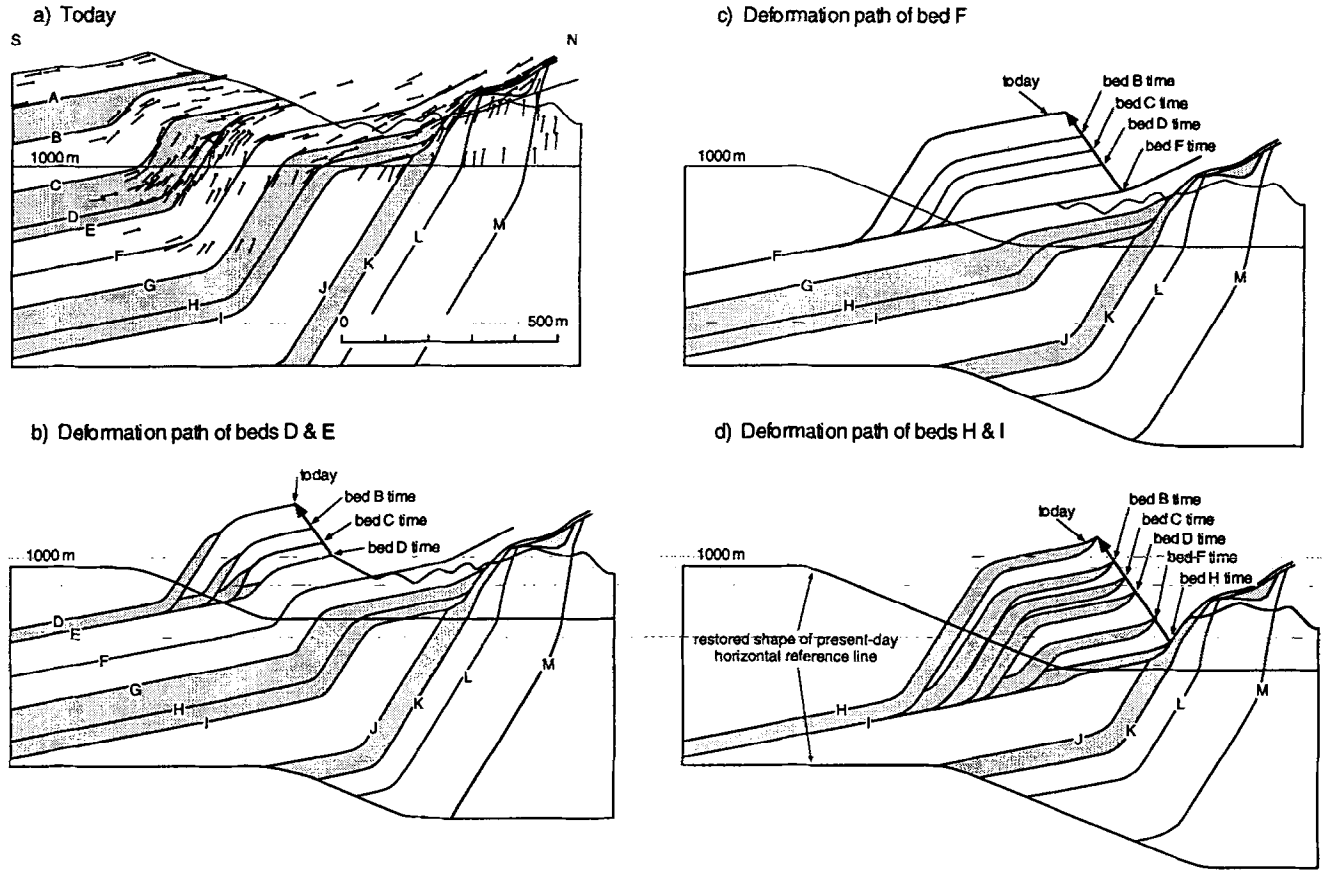

Fig. 18. Sequential deformation paths of selected horizons of the Sant Llorenç de Morunys structure, showing the history of kink-band migration (compare Fig. 1). Layer shapes are obtained from the restorations of Fig. 17.

independent of considerations of fold kinematics, such as rigid-limb rotation, kink-band migration or other more complex kinematics. The fold kinematics fall out of the restoration as a result of the spatial distribution of dips and thicknesses, which is independent of the decision that the folding vectors shall, for example, conserve layer thickness. Thus the restoration proves kink-band migration. If the last stages of fold growth at Sant Llorenç de Morunys were by rigid-limb rotation this fact would have emerged from the restoration.

DISCUSSION AND CONCLUSIONS

We have used a combination of balanced forward modeling and restoration to demonstrate that the last stages of growth of the Sant Llorenç de Morunys structure was dominated by kink-band migration of the sort that is predicted by the fault-bend fold mechanism. The complex details of the anticlinal hinge zone and associated unconformities and disconformities all have direct interpretation as effects of major fluctuations in the rates of sedimentation and deformation over a variety of timescales. At the longer timescales the average sedimentation rate varies between 200% and 50% of the uplift.

We do not have an absolute timescale for the stratigraphy so we do not know the absolute scale of these fluctuations in sedimentation and deformation. There are substantial periods during which the structure was either essentially inactive (intervals *B–C*, *E–F*, and *F–G*, Fig. 13) or deposition on the order of 100 m of conglomerate was nearly instantaneous relative to the rate of deformation. Similar fluctuations in growth are seen in the Compton–Los Alamitos fold of the Los Angeles basin, California (Shaw and Suppe, 1996). These fluctuations could be driven by climatic variation and sudden changes in the geometry of drainage basins. These fluctuations could also reflect the mechanics of a compressive structure within the larger mountain belt, governed by critical-taper wedge mechanics (Davis *et al.*, 1983; Dahlen and Suppe, 1988; Dahlen, 1990). It seems plausible that each successive earthquake in a compressive structure increases the thickness of the structure and hence progressively increases its resisting force until deformation jumps to a different, weaker structure in the mountain belt. Later, our structure may once again be the weakest structure and resume deformation. Thus structures might turn on and off on a 100,000 year timescale but be steady state on a 1–2 Ma timescale. Under this speculative scenario, the rate of deformation

within these deformational episodes may be very rapid relative to the long-term rate (see Fig. 6a). Better chronology is needed.

We have also introduced new concepts of curved-hinge kink-band migration (Figs 9 & 10) and new techniques and concepts in fold restoration (Figs 14–18) which have wider application, beyond the remarkable growth structures exposed near Sant Llorenç de Morunys (Fig. 4).

Acknowledgements—J. Suppe is exceedingly grateful for the hospitality of the people at the University of Barcelona and especially to Professor Joan Guimerà. He is also grateful for financial support from the Dirección General de Investigación Cientifica y Técnica (DGICYT) of the Spanish Ministerio de Educación y Ciencia (SAB94-0189). This paper has been partially supported by DGICYT project PB94-0908. We are grateful to Professor Oriol Riba for his introduction to the Sant Llorenç de Morunys structure and the use of his photographs. We appreciate the fruitful discussions in the field with the group from Zürich also studying the Sant Llorenç de Morunys structure, including Andrea Artoni, Mary Ford and Ed Williams (Ford *et al.*, 1997). We thank Richard W. Allmendinger, Ken McClay, and David J. Anastasio for their reviews, especially because they raised some significant issues that allowed us to clarify the role of restoration in deducing fold kinematics from the shape of growth strata.

REFERENCES

Anadón, P., Cabrera, L. Colombo, F., Marzo, M. and Riba, O. (1986) Syntectonic intraformational unconformities in alluvial fan deposits, eastern Ebro basin margin (NE Spain). In *Foreland Basins*, eds P. A. Allen and P. Homewood, Vol. 8, pp. 259–271. *Special Publication of the International Association of Sedimentologists.*

Beer, J. A., Allmendinger, R. W., Figueroa, D. E. and Jordan, T. E. (1990) Seismic stratigraphy of a Neogene piggyback basin, Argentina. *Bulletin of the American Association of Petroleum Geologists* **74**, 1183–1202.

Burbank, D. W., Vergés, J., Mu, J. A. and Bentham, P. (1992) Coeval hindward- and forward-imbricating thrusting in the central southern Pyrenees, Spain: Timing and rates of shortening and deposition. *Bulletin of the Geological Society, America* **104**, 3–17.

Burbank, D. W., Puigdefàbregas, C. and Muñoz, J. A. (1992) The chronology of the Eocene tectonic and stratigraphic development of the eastern Pyrenean foreland basin, NE Spain. *Bulletin of the Geological Society, America* **104**, 1101–1120.

Choukroune, P. and ECORS team (1989) The ECORS Pyrenean deep seismic profile reflection data and the overall structure of an orogenic belt. *Tectonics* **8**, 23–39.

Dahlen, F. A. (1990) Critical taper model of fold-and-thrust belts and accretionary wedges. *Annual Reviews of Earth and Planetary Science* **18**, 55–99.

Dahlen, F. A. and Suppe, J. (1988) Mechanics, growth and erosion of mountain belts. *Special Paper of the Geological Society, America* **218**, 161–178.

Davis, D., Suppe, J. and Dahlen, F. A. (1983) Mechanics of fold-and-thrust belts and accretionary wedges. *Journal of Geophysical Research* **88**, 1153–1172.

Erslev, E. A. (1991) Trishear fault propagation folding. *Geology* **19**, 617–620.

Epard, J. L. and Groshong, R. L. (1995) Kinematic model of detachment folding including limb rotation, fixed hinges and layer-parallel strain. *Tectonophysics* **247**, 85–103.

Fisher, D. M. and Anastasio, D. J. (1994) Kinematic analysis of a large-scale leading edge fold, Lost River Range, Idaho. *Journal of Structural Geology* **16**, 337–354.

Ford, M., Artoni, A., Williams, E. A., Vergés, J. and Hardy, S. (1997) Progressive evolution of a fault propagation fold pair from growth strata geometries, Sant Llorenç de Morunys, SE Pyrenees. *Journal of Structural Geology*, **19**, 413–441.

Hardy, S. and Poblet, J. (1994) Geometric and numerical model of progressive limb rotation in detachment folds. *Geology* **22**, 371–374.

Hedlund, C. A., Anastasio, D. J. and Fisher, D. M. (1994) Kinematics of fault-related folding in a duplex, Lost River Range, Idaho, U.S.A. *Journal of Structural Geology* **16**, 571–584.

Holl, J. E. and Anastasio, D. J. (1993) Paleomagnetically derived folding rates, southern Pyrenees, Spain. *Geology* **21**, 271–274.

Homza, T. X. and Wallace, W. K. (1995) Geometric and kinematic models for detachment folds with fixed and variable detachment depths. *Journal of Structural Geology* **17**, 575–588.

Jamison, W. R. (1987) Geometric analysis of fold development in overthrust terranes. *Journal of Structural Geology* **9**, 207–219.

Martínez, A., Vergés, J. and Muñoz, J. A. (1988) Secuencias de propagación del sistema de cabalgamientos de la terminación oriental del manto del Pedraforca y relación con los conglomerados sinorogénicos. *Acta Geologica Hispana* **23**, 119–128.

Medwedeff, D. W. (1989) Growth fault-bend folding at southeast Lost Hills, San Joaquin Valley, California. *Bulletin of the American Association of Petroleum Geologists* **73**, 54–67.

Medwedeff, D. W. (1992) Geometry and kinematics of an active, laterally propagating wedge thrust, Wheeler Ridge, California. In *Structural Geology of Fold and Thrust Belts*, eds S. Mitra and G. W. Fischer, pp. 3–28. Johns Hopkins University Press, Baltimore.

Medwedeff, D. W. and Suppe, J. (1997). Multibend fault-bend folding. *Journal of Structural Geology* **19**, 279–292.

Mueller, K. and Suppe, J. (1997). Growth of Wheeler Ridge anticline, California: implications for short-term folding behavior during earthquakes. *Journal of Structural Geology* **19**, 383–396.

Mosar, J. and Suppe, J. (1992) Role of shear in fault-propagation folding. In *Thrust Tectonics*, ed. K. R. McClay, pp. 123–132. Chapman and Hall, London.

Mount, V. S., Suppe, J. and Hook, S. C. (1990) A forward modeling strategy for balanced cross-sections. *Bulletin of the American Association of Petroleum Geologists* **74**, 521–531.

Muñoz, J. A. (1992) Evolution of a Continental Collision Belt: ECORS–Pyrenees Crustal Balanced Cross-section. In *Thrust Tectonics*, ed. K. R. McClay, pp. 235–246. Chapman and Hall, London.

Novoa, E. and Suppe, J. (1994) Solving structures caused by wedging and imbrications: Example in the northeastern Santa Barbara Channel, California. *Memorias del VII Congreso Venezolano de Geofísica*, 478–485.

Narr, W. and Suppe, J. (1994) Kinematics of basement-involved compressive structures. *American Journal of Science* **294**, 802–860.

Nunns, A. G. (1991) Structural restoration of seismic and geologic sections in extensional regimes. *Bulletin of the American Association of Petroleum Geologists* **75**, 278–297.

Poblet, J. and Hardy, S. (1995) Reverse modelling of detachment folds; application to the Pico del Aguila anticline in the south central Pyrenees (Spain). *Journal of Structural Geology* **17**, 1707–1724.

Poblet, J. and McClay, K. (1996) Geometry and kinematics of single-layer detachment folds. *Bulletin of the American Association of Petroleum Geologists* **80**, 1009–1085.

Poblet, J., Storti, F., McClay, K. and Muñoz, J. A. (1997) Geometries of syntectonic sediments associated with single-layer detachment folds. *Journal of Structural Geology* **19**, 369–381.

Pous, J., Muñoz, J. A., Ledo, J. J. and Liesa, M. (1995) Partial melting of subducted continental lower crust in the Pyrenees. *Journal of the Geological Society, London* **152**, 217–220.

Puigdefàbregas, C., Muñoz, J. A. and Marzo, M. (1986) Thrust belt development in the eastern Pyrenees and related depositional sequences in the southern foreland basin. In *Foreland Basins*, eds P. A. Allen and P. Homewood, Vol. 8, pp. 229–246. *Special Publication of the International Association of Sedimentologists.*

Puigdefàbregas, C., Muñoz, J. A. and Vergés, J. (1992) Thrusting and foreland basin evolution in the Southern Pyrenees. In *Thrust Tectonics*, ed. K. R. McClay, pp. 247–254. Chapman and Hall, London.

Riba, O. (1973) Las discordancias sintectónicas del Alto Cardener (Prepirineo catalán), ensayo de interpretación evolutiva. *Acta Geologica Hispana* **8**, 90–99.

Riba, O. (1976) Syntectonic unconformities of the Alto Cardener, Spanish Pyrenees: a genetic interpretation. *Sedimentary Geology* **15**, 213–233.

Riba, O., Reguant, S. and Villena, J. (1983) Ensayo de síntesis estratigráfica y evolutiva de la cuenca terciaria del Ebro. In *Libro Jubilar J. M. Ríos. Geología de España*, pp. 131–159. **II**. IGME, Madrid.

Shaw, J. H., Bischke, R. E. and Suppe, J. (1994a) Relationships between folding and faulting in the Loma Prieta epicentral zone: Strike-slip fault-bend folding. In: *NEHRP report to Congress, The*

Loma Prieta, California, Earthquake of October 17, 1989, pp. 3–22. *US Geological Survey Professional Paper* **1550-F**.

Shaw, J. H., Hook, S. C. and Suppe, J. (1994) Structural trend analysis by axial surface mapping. *Bulletin of the American Association of Petroleum Geologists* **78**, 700–721.

Shaw, J. H. and Suppe, J. (1994) Active faulting and growth folding in the eastern Santa Barbara Channel, California. *Bulletin of the Geological Society, America* **106**, 607–626.

Shaw, J. H. and Suppe, J. (1996) Earthquake hazards of active blind-thrust faults under the central Los Angeles basin, California. *Journal of Geophysical Research* **101**, 8623–8642.

Suppe, J. (1983) Geometry and kinematics of fault-bend folding. *American Journal of Science* **283**, 684–721.

Suppe, J. and Medwedeff, D. A. (1990) Geometry and kinematics of fault-propagation folding. *Ecolgae Geologicae Helveticae* **83**, 409–454.

Suppe, J., Chou, G. T. and Hook, S. C. (1992) Rates of folding and faulting determined from growth strata. In *Thrust Tectonics*, ed. K. R. McClay, pp. 105–121. Chapman and Hall, London.

Vergés, J. (1993) Estudi geològic del vessant sud del Pirineu oriental i central. Evolució cinemàtica en 3D. Unpublished Ph.D. thesis, University of Barcelona.

Vergés, J. and Mart, A. (1988) Corte compensado del Pirineo oriental: geometría de la cuenca de antepaís y edades de emplazamiento de los mantos de corrimiento. *Acta Geologica Hispana* **23**, 95–106.

Vergés, J. and Muñoz, J. A. (1990) Thrust sequences in the southern central Pyrenees. *Bulletin of the Geological Society, France* **8**, VI (2), 265–271.

Vergés, J. and Burbank, D. W. (1996) Eocene–Oligocene thrusting and basin configuration in the eastern and central Pyrenees (Spain). In *Tertiary Basins of Spain*, eds P. F. Friend and C. J. Dabrio, pp. 120–133. Cambridge University Press.

Vergés, J., Mill, H., Roca, E., Muñoz, J. A., Marzo, M., Cirés, J., den Bezemer, T., Zoetemeijer, R. and Cloetingh, S. (1995) Eastern Pyrenees and related foreland basins: pre-, syn- and post-collisional crustal-scale cross-sections. *Marine and Petroleum Geology* **12**, 893–915.

Vergés, J., Burbank, D. W. and Meigs, A. (1996) Unfolding: an inverse approach to fold kinematics. *Geology* **24**, 175–178.

Wickham, J. (1995) Fault displacement-gradient folds and the structure at Lost Hills, California (U.S.A.). *Journal of Structural Geology* **17**, 1293–1302.

Xiao, H. B. and Suppe, J. (1992) Origin of rollover. *Bulletin of the American Association of Petroleum Geologists* **76**, 509–529.

Zapata, T. R., and Allmendinger, R. W. (1996) Growth stratal records of instantaneous and progressive limb rotation in the Precordillera thrust belt and Bermejo basin, Argentina. *Tectonics* **15**, 1065–1083.